

Adaptive Finite-Time Attitude Tracking Control for Solar Sail with State-Dependent Torque Saturation

Liping Wu* Lu Wang** Zhihao Zhu***

* *School of Computer Engineering, Jiangsu Second Normal University,
Nanjing, China (e-mail: wulp0724@163.com).*

** *School of Automation, Nanjing University of Science and
Technology, Nanjing, China (e-mail: timwang21@126.com)*

*** *School of Electrical Engineering, Yancheng Institute of Technology,
Yancheng, China, (e-mail: zhzh@ycit.edu.cn)*

Abstract: This paper aims to investigate a fast attitude tracking control strategy for a solar sail equipped with sliding masses (SM) and roll stabilized bar (RSB) in presence of uncertain inertia, unknown disturbance, actuator saturation, and coupling between control torque and attitude angles. The state-dependent saturation of the attitude control torque is proposed to deal with the coupling between control torque and attitude angles. A novel adaptive finite-time control law is proposed to obtain fast attitude tracking, where two novel adaptive control parameters are designed to compensate the uncertain inertia, the unknown disturbance, and the state-dependent torque saturation. Compared to traditional attitude controller for solar sail, the proposed control strategy has the advantages of guaranteeing the success of actuator allocations by considering the torque constraints and of making full use of the saturated torque for fast attitude tracking. The effectiveness of the proposed control strategy is shown in a Sun-line tracking mission via simulation.

Keywords: Solar sail, Attitude control, State-dependent torque saturation, Finite-time control.

1. INTRODUCTION

Solar sail is a propellantless propulsion spacecraft that gain a continuous thrust from the solar radiation pressure (SRP) force by reflecting the sunlight via a light sail, which has gradually received increasing attention in recent years (Spencer et al., 2021; Quarta et al., 2022; Carzana et al., 2022; Pengyuan et al., 2022). The Attitude control system is particularly important for a solar sail, as its orbital acceleration is mainly controlled by the attitude of the sail. Although the attitude control torques of solar sails can be provided by traditional actuators of spacecrafts, scholars tend to design new actuators based on SRP force for the goal of propellantless propulsion. (Huang and Zhou, 2019; Yoshimura et al., 2020).

Many attitude actuators have been developed based on SRP force so far, e.g., roll stabilized bar (RSB) (Thomas et al., 2005; Wie and Murphy, 2007), sliding masses (SM) (Scholz et al., 2011; Romagnoli and Oehlschlagel, 2011; Wu et al., 2018), reflectance control device (Tian et al., 2016; Tamakoshi and Kojima, 2017; Bassetto et al., 2022), and tip vanes (Hassanpour and Damaren, 2018, 2019). In fact, only tip vanes can offer control torques along three axes, but its mechanical structure is complex and has an impact on the deployment of sail surface. Sliding masses and reflectance control device are capable of generating control torques for pitch and yaw axes, while the latter asks for high requirement of material manufacture and high financial cost. RSB generates control torque for roll

axis only, making it easy to combine with other actuators. Considering the mechanical complexity and cost, this paper takes sliding masses and RSB as actuators to study the attitude control strategy for a solar sail.

In order to achieve the desired thrust, the solar sail-based missions require fast attitude control. For example, a solar polar mission was investigated by Macdonald and Hughes (2006) and demonstrated that the sail's attitude slew rate should be at least 10deg/day. Orphee et al. (2016) pointed out that the general angular rate for sail should be 1 – 2deg/day for the NEA Scout mission of NASA. Wu and Guo (2020) focused on the effect of attitude control on the orbit maintenance of solar sail, which showed that the speed of the attitude control had a dominant effect in comparison with the attitude error boundary.

Nevertheless, a solar sail has extremely large inertia but much smaller attitude control torque than traditional spacecrafts. The magnitudes of attitude control torque that the actuators of a solar sail could offer are highly limited by their scales or structure. For the sliding masses, they change the arm of SRP force by moving masses to generate attitude control torques for yaw and pitch axes (Wie and Murphy, 2007; Bolle and Circi, 2008), and the moving distance of each mass is in proportion to the sail's scale. The RSB generates control torque for roll axis by tilting the bar's angle to adjust the SRP force, but the tilting angle is usually kept within a small boundary because of its limited mechanical structure. The

existence of torque saturation obviously poses a challenge to the attitude control of solar sail, which would result in quite a long response time of the attitude maneuver. A few of studies have investigated the attitude control considering the torque saturation for solar sail so far. Mu et al. (2015) studied attitude control for a spinning solar sail and applied a saturated function to avoid the excess of control torque after the control law design, where the stability of the system may not be guaranteed if the required control effort was beyond the saturation. Baculi and Ayoubi (2017) designed a fuzzy attitude controller for solar sail, where a control parameter was applied to modify the torque saturation, but the actuator allocation and the design of control parameter were not considered. Lian et al. (2018) proposed a saturated attitude controller for solar sail based on the adaptive sliding mode control theory where the stability analysis of the control system was given, but only the dynamics of pitch axis was taken into account.

Besides of the saturation due to the scales and mechanical structure of actuators, the attitude maneuver introduces obvious constraints on the control torque as well. For actuators designed based on SRP, e.g., sliding mass and RSB, the attitude control torques they provide are functions of SRP force and actuators' variables, while the SRP force on a sail surface is related to its attitude. The attitude adjustment of sail varies direction or magnitude of the SRP force, which in turn changes the attitude control torques. Thus, the control effort and the controlled objects are strongly coupled in attitude control of solar sail. However, studies of solar sail attitude control seldom consider this torque constraint. Actually, neglecting the coupling between attitude angles and control torques would affect the actuator allocation since the three-axis control torques are functions of both the attitude angles and the actuators' variables. Lian et al. (2018) choose the torque saturation as the maximum value that the actuator could offer with attitude angle of 90 degree, and assumed that the actuator should be always ready for the maximum torque for any other attitude, but the solutions of actuators' variables may not always exist for the required torque. The potential failure in actuator allocation would also damage the stability of attitude control system due to the considerable error between the controller's output and the affordable torque from the actuator system.

Furthermore, the sliding masses adjust the offset between center of mass(CM) and center of pressure(CP) by changing the mass center of solar sail, which leads to a time-varying inertia. Meanwhile, there usually exists an inherent CM/CP offset due to the manufacturing error or uncertainties in sail's deployment (Wie and Murphy, 2007; Adeli et al., 2011), which introduces an unknown SRP disturbance torque to the attitude control system. For such uncertainties and unknown disturbances, a control strategy with high robustness and efficient adaptability is required for solar sail equipped with sliding masses and RSB. Nevertheless, most researches on solar sail's attitude control tend to focus on the dynamics studies of specific actuator (Gong and Li, 2015; Eldad and Lightsey, 2015; Niccolai et al., 2017) but less on the control strategy investigation for the uncertainties and unknown disturbances in practice, especially for that with sliding masses and RSB.

Considering the aforementioned issues, this paper aims to develop a finite time attitude controller for solar sail due to its good performance in fast convergence and the wide applications in attitude control of spacecraft (Zhong et al., 2016; Hu and Tan, 2017; Zhu and Guo, 2017; Zhu et al., 2019), to obtain a fast tracking control of sail's attitude required by orbit mission. A solar sail equipped with sliding masses and RSB is investigated, taking into account the changing inertia, the unknown SRP disturbance, as well as the torque constraints caused by actuator saturation and attitude maneuver. The remain is organized as follows. Section 2 gives the mathematical preliminaries, and establishes the mathematical model of control torque with respect to attitude angle. Section 3 proposes the design of control strategy and gives the stability analysis. Numerical simulation is given in Section 4. The conclusions are drawn in Section 5.

2. MATHEMATICAL PRELIMINARIES

2.1 Attitude Models

Consider a square solar sail like the one shown in Fig. 1, where the sail is assumed to be flat and the degradation of the sail membrane is not taken into account. Define S_I as an inertia frame and $S_b(o x_b y_b z_b)$ as a body-fixed frame. In particular, o is the geometrical centre of sail, x_b (the roll axis) is along with the normal vector of sail, pointing towards Sun, y_b (the pitch axis) is along with one of the diagonal line of sail, and z_b (the yaw axis) forms the right handed frame.

To avoid the singularity, the quaternion is used to describe the attitude of solar sail. The attitude dynamics in body frame is given by

$$\mathbf{J}\dot{\boldsymbol{\omega}} + \boldsymbol{\omega}^\times \mathbf{J}\boldsymbol{\omega} = \boldsymbol{\tau}_c + \boldsymbol{\tau}_d \quad (1)$$

$$\dot{\mathbf{Q}} = \frac{1}{2} \begin{bmatrix} q_4 \mathbf{I}_3 + \mathbf{q}^\times \\ -\mathbf{q}^T \end{bmatrix} \boldsymbol{\omega} \quad (2)$$

where $\boldsymbol{\omega} \in \mathbb{R}^3$ is the angular velocity of the solar sail with respect to frame S_I described in frame S_b , $\mathbf{J} \in \mathbb{R}^{3 \times 3}$ is the inertia matrix, $\mathbf{Q} = [q^T, q_4]^T$, with $\mathbf{q} = [q_1, q_2, q_3]^T$ and satisfying $\|\mathbf{Q}\| = 1$, represents the orientation of frame S_b with respect to frame S_I , $\mathbf{I}_3 \in \mathbb{R}^{3 \times 3}$ is the identity matrix. The operator \times for any vector $\mathbf{a} = [a_1, a_2, a_3]^T$ is

$$\mathbf{a}^\times = \begin{bmatrix} 0 & -a_3 & a_2 \\ a_3 & 0 & -a_1 \\ -a_2 & a_1 & 0 \end{bmatrix}$$

so that the following property holds: $\|\mathbf{a}^\times\| = \|\mathbf{a}\|$.

Following Thomas et al. (2005) and Wie and Murphy (2007), the attitude control torque generated by two sliding masses and RSB system can be described as

$$\boldsymbol{\tau}_c = \begin{bmatrix} \frac{\sqrt{2}}{3} l_b F_s \sin \frac{\alpha_b}{2} - \frac{m}{M} (F_z d_y - F_y d_z) \\ -\frac{m}{M} d_z F_x \\ \frac{m}{M} d_y F_x \end{bmatrix} \quad (3)$$

where, l_b is the length of RSB, α_b is the tilting angle of RSB, d_y and d_z are the trim positions of the sliding masses on the pitch and yaw axes, respectively, α_b , d_y , and d_z are the so-called actuators' variables, F_s is the norm of SRP force, F_x , F_y , and F_z are the roll, pitch, and yaw components of SRP force in body frame, respectively, M

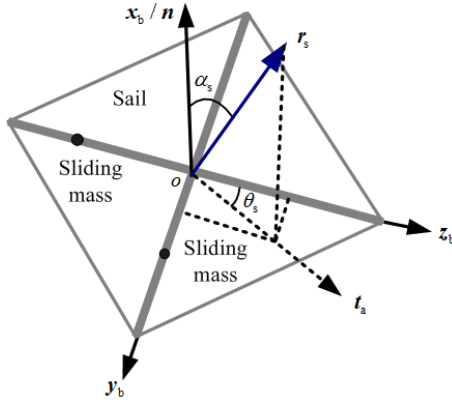


Fig. 1. Square Solar Sail

is the total mass of the solar sail and m is the mass of each sliding mass.

Due to the limitations from RSB's structure and sail's scale, the actuators' variables are subject to

$$\begin{cases} |\alpha_b| \leq \alpha_{bm} \\ |d_y| \leq d_m \\ |d_z| \leq d_m \end{cases} \quad (4)$$

where α_{bm} is the maximum rotational angle of the RSB and d_m is the maximum moving distance of each sliding mass.

The components of the inertia matrix change when the sliding masses move and are given by

$$\begin{cases} J_x = J_{x0} + m_r(d_y^2 + d_z^2) \\ J_y = J_{y0} + m_r d_z^2 \\ J_z = J_{z0} + m_r d_y^2 \end{cases} \quad (5)$$

where J_{x0} , J_{y0} , and J_{z0} are the principal inertia moments of solar sail with sliding masses fixed at their initial positions, and m_r is the so-called reduced mass, defined as

$$m_r = \frac{m(M - m)}{M} \quad (6)$$

Actually, the inertia can be denoted as $\mathbf{J} = \mathbf{J}_0 + \Delta\mathbf{J}$, where

$$\mathbf{J}_0 = [J_{x0}, J_{y0}, J_{z0}]^T \quad (7)$$

$$\Delta\mathbf{J} = [m_r(d_y^2 + d_z^2), m_r d_z^2, m_r d_y^2]^T \quad (8)$$

The disturbance torque due to CM/CP offset can be written as (Adeli et al. (2011))

$$\boldsymbol{\tau}_d = \boldsymbol{\iota}_0 \times \mathbf{F}_{sb} \quad (9)$$

where $\boldsymbol{\iota}_0 = [0, \iota_{0y}, \iota_{0z}]^T$ is the inherent CM/CP offset vector and $\mathbf{F}_{sb} = [F_x, F_y, F_z]^T$ is the SRP force described in the body frame.

2.2 Constraints of attitude control torque

From Eq.(3), it can be seen that the attitude control torque is not only changed by the varying distances of the sliding masses (d_z/d_y) and by the rotational angle of RSB (α_b), but it is also limited by the SRP force, which is adjusted by solar sail's attitude. Thus, the attitude maneuver would also change the attitude control torque. Here, the mathematical model is provided for the description of attitude control torque in terms of the attitude angles of solar sail.

Two attitude angles, the so-called Sun angle and clock angle, are usually defined for solar sails, see Fig 1. In particular, α_s is the Sun angle, that is the angle between sail's normal vector (\mathbf{n}) and the sunlight vector (\mathbf{r}_s), while θ_s is the clock angle, defined as the angle between the projection of the sunlight vector in $y_b o_b z_b$ plane and the z_b axis.

The SRP force can be decomposed along the normal vector and the tangential vector which is denoted as \mathbf{t}_a , that is(Adeli et al. (2011))

$$\mathbf{F}_{srp} = F_n \mathbf{n} + F_t \mathbf{t}_a \quad (10)$$

with

$$F_n = -PA_s[(1 + \rho_s)\cos^2 \alpha_s + 2/3\rho_d \cos \alpha_s] \quad (11)$$

$$F_t = -PA_s(1 - \rho_s)\cos \alpha_s \sin \alpha_s \quad (12)$$

where A_s is the effective area of sail, P is the value of SPR at 1 astronomical unit from the Sun, ρ_s is the specular reflection coefficient, and ρ_d is the diffuse reflection coefficient. The optical parameters are assumed to be constant.

The SRP force described in S_b is

$$\mathbf{F}_{sb} = \begin{bmatrix} F_n \\ F_t \sin \theta_s \\ F_t \cos \theta_s \end{bmatrix} \quad (13)$$

Substituting Eqs.(11) and (12) into Eq.(13), yields

$$F_x = -PA_s[(1 + \rho_s)\cos^2 \alpha_s + 2/3\rho_d \cos \alpha_s] \quad (14)$$

$$F_y = -PA_s(1 - \rho_s)\cos \alpha_s \sin \alpha_s \sin \theta_s \quad (15)$$

$$F_z = -PA_s(1 - \rho_s)\cos \alpha_s \sin \alpha_s \cos \theta_s \quad (16)$$

Thereafter, F_x , F_y , and F_z are substituted into Eq.(3), thus giving

$$\boldsymbol{\tau}_c = \begin{bmatrix} \frac{\sqrt{2}}{3} l_b F_s \sin \frac{\alpha_b}{2} + \frac{m}{M} F_o (\cos \theta_s d_y - \sin \theta_s d_z) \\ \frac{m}{M} P A_s d_z [(1 + \rho_s) \cos \alpha_s + 2/3\rho_d] \cos \alpha_s \\ -\frac{m}{M} P A_s d_y [(1 + \rho_s) \cos \alpha_s + 2/3\rho_d] \cos \alpha_s \end{bmatrix} \quad (17)$$

where $F_o = PA_s(1 - \rho_s)\cos \alpha_s \sin \alpha_s$.

It is clearly shown that the three-axes control torques are nonlinear functions of the two attitude angles and actuators' variables. The changes in Sun and clock angles during the attitude maneuver introduce obvious constraints on the control torque.

Note that α_s and θ_s can be calculated as

$$\cos \alpha_s = \mathbf{r}_{sb} \cdot \mathbf{x}_b \quad (18)$$

$$\begin{cases} \sin \theta_s = \frac{\mathbf{r}_{sb}(2)}{\sqrt{\mathbf{r}_{sb}^2(2) + \mathbf{r}_{sb}^2(3)}}, \alpha_s \neq 0 \\ \theta_s = 0, \alpha_s = 0 \end{cases} \quad (19)$$

where θ_s is set to zero when $\alpha_s = 0$ for the calculation logic.

The sunlight vector in frame S_I can be transformed from its description in S_b as

$$\mathbf{r}_{sb} = \mathbf{A}_{bI} \mathbf{r}_{sI} \quad (20)$$

where \mathbf{A}_{bI} is the transform matrix from S_I to S_b , which can be described by the attitude quaternions as

$$\mathbf{A}_{bI} = \begin{bmatrix} 1 - 2q_2^2 - 2q_3^2 & 2q_1q_2 + q_4q_3 & 2q_1q_3 - q_4q_2 \\ 2q_1q_2 - q_4q_3 & 1 - 2q_1^2 - 2q_3^2 & 2q_2q_3 - q_4q_1 \\ 2q_1q_3 + q_4q_2 & 2q_2q_3 - q_4q_1 & 1 - 2q_1^2 - 2q_2^2 \end{bmatrix} \quad (21)$$

Thus, the transformation from attitude quaternions to attitude angles is obtained.

From Eq.(4)-(8), it can be seen that the inertia changing with respect to the positions of sliding masses is bounded. Meanwhile, the SRP disturbance torque is bounded due to the limited area of sail, see Eqs.(9)-(16). As a consequence, the following assumptions can be given.

Assumption 1. There exist $b_J > 0$, $b_{J1} > 0$, and $b_{J2} > 0$ such that $b_{J1} \leq \|J_0\| \leq b_J$ and $\|\Delta J\| \leq b_{J2}$, where b_J , b_{J1} , and b_{J2} are unknown.

Assumption 2. The SRP disturbance torque is bounded such that $\|\tau_d\| \leq d_s$, where $d_s > 0$ is unknown.

2.3 Definition and lemma

The definition of practical finite-time stable (PFS) and lemma of finite-time control are introduced, which will be utilized in the design of the attitude controller.

Definition 1. (Zhu et al. (2011)) Consider the nonlinear system $\dot{\mathbf{x}} = \mathbf{f}(\mathbf{x}, \mathbf{u})$, where \mathbf{x} is a state vector and \mathbf{u} is the input vector. The solution is practical finite-time stable (PFS) if for all $x(t_0) = x_0$, there exist $\varepsilon > 0$ and $T(\varepsilon, x_0) < \infty$, such that $\|x(t)\| < \varepsilon$, for all $t \leq t_0 + T$, where t_0 is the initial time.

Lemma 1. (Zhu et al. (2011)) Consider the nonlinear system $\dot{\mathbf{x}} = \mathbf{f}(\mathbf{x}, \mathbf{u})$, where \mathbf{x} is a state vector and \mathbf{u} is the input vector. Suppose that there exist continuous function $V(x)$, scalars $\alpha > 0$, $0 < \gamma < 1$, and $0 < \beta < \infty$ such that

$$\dot{V}(x) \leq -\alpha V^\gamma(x) + \beta \quad (22)$$

Then, the trajectory of system $\dot{\mathbf{x}} = \mathbf{f}(\mathbf{x}, \mathbf{u})$ is PFS. The decrease of $V(x)$ drives the trajectory of the system into

$$V^\gamma(x) \leq \frac{\beta}{\alpha(1-\kappa)}, \quad \kappa \in (0, 1) \quad (23)$$

and the needed time is bounded by

$$T \leq \frac{V^{1-\gamma}(\mathbf{x}_0)}{\alpha\kappa(1-\gamma)} \quad (24)$$

where \mathbf{x}_0 is the initial state of the system.

2.4 Error model

To describe the attitude tracking problem for solar sail, another frame \mathbf{S}_d is defined to describe the desired attitude of solar sail. In particular, the orientation of \mathbf{S}_d with respect to \mathbf{S}_I is described by $\mathbf{Q}_d = [q_d^T, q_{d4}]^T$, where $\mathbf{q}_d = [q_{d1}, q_{d2}, q_{d3}, q_{d4}]^T$ satisfies $\|\mathbf{Q}_d\| = 1$. Let $\boldsymbol{\omega}_d \in \mathbf{R}^3$ denotes the desired angular velocity described in \mathbf{S}_d , equivalent to the angular velocity of \mathbf{S}_d with respect to \mathbf{S}_I . In addition, $\mathbf{Q}_e = [q_e^T, q_{e4}]^T = [q_{e1}, q_{e2}, q_{e3}, q_{e4}]^T$, satisfying $\|\mathbf{Q}_e\| = 1$, is defined to describe the rotation from \mathbf{S}_d to \mathbf{S}_b , while $\boldsymbol{\omega}_e \in \mathbf{R}^3$ describes the angular velocity of \mathbf{S}_b relative to \mathbf{S}_d in \mathbf{S}_b . The transformation matrix from \mathbf{S}_d to \mathbf{S}_b is denoted by $\mathbf{C} \in \mathbf{R}^{3 \times 3}$, where

$$\mathbf{C} = (q_4^2 - \mathbf{q}_e^T \mathbf{q}_e) \mathbf{I}_3 + \mathbf{q}_e \mathbf{q}_e^T - 2q_4 \mathbf{q}_e^\times \quad (25)$$

is such that $\|\mathbf{C}\| = 1$, and $\dot{\mathbf{C}} = -\boldsymbol{\omega}_e^\times \mathbf{C}$. The quaternion error is

$$\mathbf{q}_e = q_{d4} \mathbf{q} - \mathbf{q}_d^\times \mathbf{q} - q_4 \mathbf{q}_d \quad (26)$$

$$q_{e4} = \mathbf{q}^T \mathbf{q}_d + q_4 q_{d4} \quad (27)$$

$$\boldsymbol{\omega}_e = \boldsymbol{\omega} - \mathbf{C} \boldsymbol{\omega}_d \quad (28)$$

Substituting Eq.(28) into Eq.(1), it has

$$\mathbf{J} \dot{\boldsymbol{\omega}}_e = -(\boldsymbol{\omega}_e + \mathbf{C} \boldsymbol{\omega}_d)^\times \mathbf{J}(\boldsymbol{\omega}_e + \mathbf{C} \boldsymbol{\omega}_d) + \mathbf{J}(\boldsymbol{\omega}_e^\times \mathbf{C} \boldsymbol{\omega}_d - \mathbf{C} \dot{\boldsymbol{\omega}}_d) + \boldsymbol{\tau}_c + \boldsymbol{\tau}_d \quad (29)$$

The following error model of dynamics can be obtained

$$\begin{aligned} \mathbf{J}_0 \dot{\boldsymbol{\omega}}_e = & -(\boldsymbol{\omega}_e + \mathbf{C} \boldsymbol{\omega}_d)^\times \mathbf{J}_0(\boldsymbol{\omega}_e + \mathbf{C} \boldsymbol{\omega}_d) + \\ & \mathbf{J}_0(\boldsymbol{\omega}_e^\times \mathbf{C} \boldsymbol{\omega}_d - \mathbf{C} \dot{\boldsymbol{\omega}}_d) + \boldsymbol{\tau}_c + \boldsymbol{\tau}_d - \Delta \mathbf{J} \boldsymbol{\omega}_e \\ & - (\boldsymbol{\omega}_e + \mathbf{C} \boldsymbol{\omega}_d)^\times \Delta \mathbf{J}(\boldsymbol{\omega}_e + \mathbf{C} \boldsymbol{\omega}_d) + \\ & \Delta \mathbf{J}(\boldsymbol{\omega}_e^\times \mathbf{C} \boldsymbol{\omega}_d - \mathbf{C} \dot{\boldsymbol{\omega}}_d) \end{aligned} \quad (30)$$

and the error model of kinematics is

$$\dot{\mathbf{Q}}_e = \frac{1}{2} \begin{bmatrix} q_{e4} \mathbf{I}_3 + \mathbf{q}_e^\times \\ -\mathbf{q}_e^T \end{bmatrix} \boldsymbol{\omega}_e \quad (31)$$

Since the desired angular velocity required by the orbital mission of solar sail is usually bounded, the following assumption can be given.

Assumption 3. The desired attitude angular velocity and its time derivative are bounded. There exist unknown $v_i > 0$, with $i = 1, 2$ that satisfy $\|\boldsymbol{\omega}_d\| \leq v_1$, and $\|\dot{\boldsymbol{\omega}}_d\| \leq v_2$.

Therefore, the control objective is to design an attitude tracking controller for solar sail described by Eqs.(1) and (2) in presence of the actuator saturation limitations described by Eq.(4), the uncertain inertia described by Eq.(5), the SRP disturbance torque given by Eq.(9), and the control torque subject to Eq.(17) under the Assumptions 1-3. With the designed attitude controller, the attitude angular error and the angular velocity error described by Eqs.(30) and (31) are PFS.

3. CONTROL STRATEGY DESIGN

The attitude tracking controller is designed in this section. A state-dependent torque saturation is firstly proposed to deal with the constants of attitude control torque of solar sail, and then the adaptive finite-time control law is designed. The actuator allocation is thereafter studied. Fig. 2 shows the block diagram of the control system, where \mathbf{u}_s is the control law, α_{bc} is the reference command of RSB's rotational angle, d_{yc} and d_{zc} are reference commands of sliding masses' positions, while α_{bc} , d_{yc} and d_{zc} are solved from \mathbf{u}_s in actuator allocation.

3.1 State-dependent torque saturation

Firstly, the torque constraints are considered. Baculi and Ayoubi (2017) proposed a control parameter to change the actuator's saturation to adjust the attitude control performance of solar sail. Inspired by the idea, a state-dependent torque saturation is proposed to combine the torque constraints of actuator saturation and attitude maneuver. In detail, the influence of attitude maneuver is equivalent to the saturation of control torque.

Most orbit missions of solar sail are dependent on the Sun angle (Adeli et al., 2011; Wie and Murphy, 2007; Macdonald and Hughes, 2006; Heiligers et al., 2015), therefore the item of the clock angle (θ_s) in Eq. (17) can be ignored to simplify the controller design, thus yielding

$$\boldsymbol{\tau}_{c1} = \begin{bmatrix} \frac{\sqrt{2}}{3} l_b F_s \sin \frac{\alpha_b}{2} \\ \frac{m}{M} P A_s d_z [(1 + \rho_s) \cos \alpha_s + 2/3 \rho_d] \cos \alpha_s \\ -\frac{m}{M} P A_s d_y [(1 + \rho_s) \cos \alpha_s + 2/3 \rho_d] \cos \alpha_s \end{bmatrix} \quad (32)$$

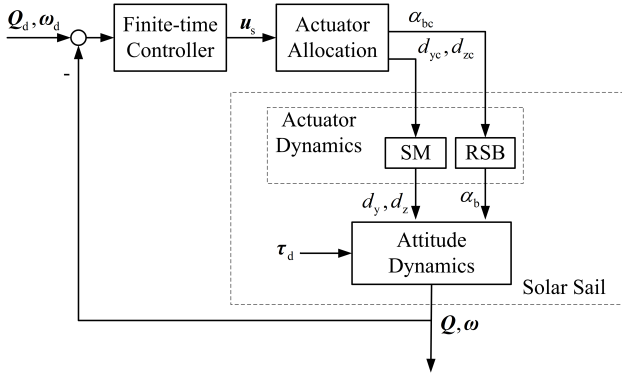


Fig. 2. Diagram of control system

The equals are taken in Eq. (4) to use the maximum values of actuators' variables. Thus, the saturation of the control torque can be obtained by substituting α_{bm} and d_m into Eq. (32) as

$$\mathbf{U}_m = \begin{bmatrix} \frac{\sqrt{2}}{3} l_b F_s \sin \frac{\alpha_b}{2} \\ \frac{m_F}{M} P A_s d_m [(1 + \rho_s) \cos \alpha_s + 2/3 \rho_d] \cos \alpha_s \\ \frac{m_F}{M} P A_s d_m [(1 + \rho_s) \cos \alpha_s + 2/3 \rho_d] \cos \alpha_s \end{bmatrix} \quad (33)$$

which gives the torque saturation as a function of the Sun angle.

3.2 Finite-time Attitude Tracking Law

The attitude control law is designed based on the fast terminal sliding mode finite-time control theory for its good performance in fast convergence. Two adaptive parameters are proposed to compensate the uncertain inertia, the unknown SRP disturbance, and the state-dependent torque saturation.

The following sliding surface is applied

$$\mathbf{s} = \boldsymbol{\omega}_e + c_1 \mathbf{q}_e + c_2 \mathbf{F}(\mathbf{q}_e, r) \quad (34)$$

where $c_1 > 0, c_2 > 0, r = g/h$, g and h are two positive odd numbers satisfying $g/h \in (0, 1)$. For any vector $\mathbf{x} = [x_1, x_2, x_3]^T$ and any scalar v , the function $\mathbf{F}(\mathbf{x}, v)$ is

$$\mathbf{F}(\mathbf{x}, v) = [|x_1|^v \text{sign}(x_1), |x_2|^v \text{sign}(x_2), |x_3|^v \text{sign}(x_3)]^T \quad (35)$$

To reduce the number of estimated parameters, the following lumped disturbance item is defined

$$\mathbf{D} = \boldsymbol{\tau}_d - \Delta \mathbf{J} \dot{\boldsymbol{\omega}}_e + \Delta \mathbf{J} (\boldsymbol{\omega}_e^\times \mathbf{C} \boldsymbol{\omega}_d - \mathbf{C} \dot{\boldsymbol{\omega}}_d) - (\boldsymbol{\omega}_e + \mathbf{C} \boldsymbol{\omega}_d)^\times \Delta \mathbf{J} (\boldsymbol{\omega}_e + \mathbf{C} \boldsymbol{\omega}_d) \quad (36)$$

The following theorem can be given

Theorem 1. Considering the attitude system in Eqs.(1)-(2) subject to the control torque in Eq.(17) and to the actuator saturation in Eq.(4) with Assumptions 1-2, there exists $a > 0$ such that

$$\|\dot{\boldsymbol{\omega}}\| \leq \|\boldsymbol{\omega}\|^2 + a \quad (37)$$

Proof. According to Eq. (1), it has

$$\begin{aligned} \|\mathbf{J}\|\|\dot{\boldsymbol{\omega}}\| &= \|-\boldsymbol{\omega}^\times \mathbf{J} \boldsymbol{\omega} + \boldsymbol{\tau}_c + \boldsymbol{\tau}_d\| \\ &\leq \|\boldsymbol{\omega}^\times \mathbf{J} \boldsymbol{\omega}\| + \|\boldsymbol{\tau}_c\| + \|\boldsymbol{\tau}_d\| \\ &\leq \|\mathbf{J}\|\|\boldsymbol{\omega}\|^2 + d_s + \|\boldsymbol{\tau}_c\| \end{aligned} \quad (38)$$

From Eq.(17), the control torque components are the trigonometric functions of Sun angle and actuators' variables. The trigonometric functions of Sun angle are

bounded, and the actuators' variables are saturated as described by Eq.(4). Thus, the control torque is bounded and the boundary can be denoted as

$$\|\boldsymbol{\tau}_c\| \leq a_0, \quad a_0 > 0 \quad (39)$$

from which

$$\|\mathbf{J}\|\|\dot{\boldsymbol{\omega}}\| \leq \|\mathbf{J}\|\|\boldsymbol{\omega}\|^2 + d_s + a_0 \quad (40)$$

and

$$\|\dot{\boldsymbol{\omega}}\| \leq \|\boldsymbol{\omega}\|^2 + (d_s + a_1)/b_{J1} \quad (41)$$

Define $a =: (d_s + a_1)/b_{J1}$, thus having

$$\|\dot{\boldsymbol{\omega}}\| \leq \|\boldsymbol{\omega}\|^2 + a \quad (42)$$

The following theorem can also be given according to Theorem 1.

Theorem 2. Considering the lumped disturbance given by Eq.(36) that satisfies Assumptions 1-3, there exist $a_i > 0$, with $i = 1, 2, 3$, such that the following inequality holds

$$\|\mathbf{D}\| \leq a_1 \|\boldsymbol{\omega}\|^2 + a_2 \|\boldsymbol{\omega}\| + a_3 \quad (43)$$

Proof. From Eq.(36), it has

$$\begin{aligned} \|\mathbf{D}\| &\leq \|\boldsymbol{\tau}_d\| + \|\Delta \mathbf{J}\|\|\dot{\boldsymbol{\omega}}\| + \mathbf{C} \dot{\boldsymbol{\omega}}_d + \dot{\mathbf{C}} \boldsymbol{\omega}_d + \|\Delta \mathbf{J}\|(\|\boldsymbol{\omega}_e\| \\ &\quad \|\boldsymbol{\omega}_d\| + \|\dot{\boldsymbol{\omega}}_d\|) + \|\Delta \mathbf{J}\|\|\boldsymbol{\omega}\|^2 \\ &\leq d_s + \|\Delta \mathbf{J}\|\|\dot{\boldsymbol{\omega}}\| + \|\Delta \mathbf{J}\|\|\boldsymbol{\omega}\|^2 + 2\|\Delta \mathbf{J}\|(\|\boldsymbol{\omega}_d\| \\ &\quad + \|\boldsymbol{\omega}_e\|\|\boldsymbol{\omega}_d\|) \\ &\leq d_s + \|\Delta \mathbf{J}\|\|\dot{\boldsymbol{\omega}}\| + 2\|\Delta \mathbf{J}\|\|\boldsymbol{\omega}_d\|\|\boldsymbol{\omega}\| + \|\Delta \mathbf{J}\|\|\boldsymbol{\omega}\|^2 \\ &\quad + 2\|\Delta \mathbf{J}\|\|\boldsymbol{\omega}_d\|^2 + 2\|\Delta \mathbf{J}\|\|\boldsymbol{\omega}_d\| \end{aligned} \quad (44)$$

According to Theorem 1, it has

$$\begin{aligned} \|\mathbf{D}\| &\leq \|\Delta \mathbf{J}\|(\|\boldsymbol{\omega}\|^2 + a) + 2\|\Delta \mathbf{J}\|\|\boldsymbol{\omega}_d\|\|\boldsymbol{\omega}\| + d_s + \\ &\quad \|\Delta \mathbf{J}\|\|\boldsymbol{\omega}\|^2 + 2\|\Delta \mathbf{J}\|\|\boldsymbol{\omega}_d\|^2 + 2\|\Delta \mathbf{J}\|\|\boldsymbol{\omega}_d\| \\ &= 2\|\Delta \mathbf{J}\|\|\boldsymbol{\omega}\|^2 + 2\|\Delta \mathbf{J}\|\|\boldsymbol{\omega}_d\|\|\boldsymbol{\omega}\| + d_s \\ &\quad + 2\|\Delta \mathbf{J}\|\|\boldsymbol{\omega}_d\|^2 + 2\|\Delta \mathbf{J}\|\|\boldsymbol{\omega}_d\| \end{aligned} \quad (45)$$

From Assumptions 1 and 2, a_1, a_2 , and a_3 can be always found such that

$$a_1 \geq 2\|\Delta \mathbf{J}\| \quad (46)$$

$$a_2 \geq 2\|\Delta \mathbf{J}\|\|\boldsymbol{\omega}_d\| \quad (47)$$

$$a_3 \geq d_s + 2\|\Delta \mathbf{J}\|\|\boldsymbol{\omega}_d\|^2 + 2\|\Delta \mathbf{J}\|\|\boldsymbol{\omega}_d\| \quad (48)$$

then yields

$$\|\mathbf{D}\| \leq a_1 \|\boldsymbol{\omega}\|^2 + a_2 \|\boldsymbol{\omega}\| + a_3 \quad (49)$$

The following assumption can also be given

Assumption 4. There exist $p_1 > 0$ and $p_2 > 0$ such that the following inequalities hold

$$c_1 \|\mathbf{q}_e\| + c_2 \|\mathbf{q}_e\|^r + \frac{c_2}{2} \|\mathbf{q}_e\|^{r-1} + 2\|\boldsymbol{\omega}_d\| + \frac{c_1}{2} \leq \frac{p_1}{b_J} \quad (50)$$

$$\|\dot{\boldsymbol{\omega}}_d\| + \left(\frac{c_1}{2} + \frac{c_2}{2} r \|\mathbf{q}_e\|^{r-1}\right) \leq \frac{p_2}{b_J} \quad (51)$$

Since the desired angular velocity and its derivative are bounded from Assumption 3, and the error quaternion is subject to $\|\mathbf{Q}_e\| = 1$, Assumption 4 is reasonable.

Theorem 2 and Assumption 4 combine the information about the inertia, the SRP disturbance, and the saturation of attitude control torque, which aims to reduce the number of estimated parameters.

For further reduction, it denotes

$$p = \max(p_1, p_2) \quad (52)$$

$$d = \max(a_1, a_2, a_3) \quad (53)$$

Thus, only two adaptive parameters, d and p , are applied in the proposed controller, which are updated online as the following laws

$$\dot{d} = \eta_0(\Phi_0 \|s\| - \epsilon_0 \hat{d}) \quad (54)$$

$$\dot{p} = \eta_1(\Phi_1 \|s\| - \epsilon_1 \hat{p}) \quad (55)$$

where $\Phi_0 = 1 + \|\omega\| + \|\omega\|^2$, $\Phi_1 = 1 + \|\omega\|$, $\epsilon_0 > 0$, and $\epsilon_1 > 0$. η_0 and η_1 are positive numbers which will be determined in following control law design.

The saturated control law is designed as

$$\mathbf{u}_s = -\chi(\mathbf{u})\mathbf{u} \quad (56)$$

where $\chi = \text{diag}[\chi_1, \chi_2, \chi_3]$ is used to avoid the excess of attitude control torque, and

$$\chi_i = \begin{cases} 1, & |u_i| \leq U_{mi} \\ U_{mi}/u_i \text{sign}(u_i), & \text{otherwise} \end{cases}, \text{ with } i = 1, 2, 3 \quad (57)$$

\mathbf{u} is the finite-time control law designed as

$$\mathbf{u} = k_1 \mathbf{s} + k_2 \mathbf{F}(\mathbf{s}, r) + \mathbf{u}_{ad}(\mathbf{s}, \hat{d}, \hat{p}) \quad (58)$$

where $k_1 > 0, k_2 > 0$, and $\mathbf{u}_{ad}(\mathbf{s}, \hat{d}, \hat{p})$ is the adaptive law and designed as

$$\mathbf{u}_{ad}(\mathbf{s}, \hat{d}, \hat{p}) = \begin{cases} \frac{\mathbf{s}}{\|\mathbf{s}\|} \hat{d} \Phi_0 + \frac{\mathbf{s}}{\|\mathbf{s}\|} \hat{p} \Phi_1, & \|\mathbf{s}\| \geq \sigma \\ \frac{\sigma}{\sigma} \hat{d} \Phi_0 + \frac{\sigma}{\sigma} \hat{p} \Phi_1, & \|\mathbf{s}\| < \sigma \end{cases} \quad (59)$$

where $\sigma > 0$.

The stability of the closed-loop system based on the proposed control law is given in following theorem.

Theorem 3. Consider the system described by Eqs.(1)-(2) that satisfies Assumptions 1-4 with the actuator saturation in Eq.(4), the uncertain inertia in Eq.(5), the SRP disturbance torque in Eq.(9), and the torque constraint in Eq.(17). Then, the attitude error \mathbf{q}_e and the angular velocity error ω_e defined in Eq.(30) and Eq.(31) are PFS with the control laws (56)-(58) and the adaptive laws (59), (54)-(55).

Proof. According to Lu et al. (2013), there exists a constant satisfying that $0 < \delta \leq \min(\chi_i) \leq 1$, while the following Lyapunov function is chosen

$$V = \frac{1}{2} \left(\mathbf{s}^T \mathbf{J}_0 \mathbf{s} + \frac{1}{\eta_0 \delta} \tilde{d}^2 + \frac{1}{\eta_1 \delta} \tilde{p}^2 \right) \quad (60)$$

where $\tilde{d} = d - \delta \hat{d}$, $\tilde{p} = p - \delta \hat{p}$. Its derivative is

$$\begin{aligned} \dot{V} &= \mathbf{s}^T \mathbf{J}_0 \dot{\mathbf{s}} - \frac{1}{\eta_0} (d - \delta \hat{d}) \dot{\tilde{d}} - \frac{1}{\eta_1} (p - \delta \hat{p}) \dot{\tilde{p}} \\ &= \mathbf{s}^T [\mathbf{J}_0 \dot{\omega}_e + c_1 \mathbf{J}_0 \dot{\mathbf{q}}_e + c_2 r \mathbf{J}_0 \text{diag}(|\mathbf{q}_e|^{r-1}) \dot{\mathbf{q}}_e] \\ &\quad - \frac{1}{\eta_0} (d - \delta \hat{d}) \dot{\tilde{d}} - \frac{1}{\eta_1} (p - \delta \hat{p}) \dot{\tilde{p}} \\ &= \mathbf{s}^T [-\omega_e^\times \mathbf{J}_0 \omega + \mathbf{J}_0 (\omega_e^\times \mathbf{C} \omega_d - \mathbf{C} \dot{\omega}_d) + c_1 \mathbf{J}_0 \dot{\mathbf{q}}_e \\ &\quad + c_2 r \mathbf{J}_0 \text{diag}(|\mathbf{q}_e|^{r-1}) \dot{\mathbf{q}}_e] + \tau_c + \mathbf{D} \\ &\quad - \frac{1}{\eta_0} (d - \delta \hat{d}) \dot{\tilde{d}} - \frac{1}{\eta_1} (p - \delta \hat{p}) \dot{\tilde{p}} \\ &= \mathbf{s}^T [-(\mathbf{s} - c_1 \mathbf{q}_e - c_2 \mathbf{F}(\mathbf{q}_e, r) + \mathbf{C} \omega_d)^\times \mathbf{J}_0 \omega + \mathbf{J}_0 \\ &\quad (\omega_e^\times \mathbf{C} \omega_d - \mathbf{C} \dot{\omega}_d) + c_1 \mathbf{J}_0 \dot{\mathbf{q}}_e + c_2 r \mathbf{J}_0 \text{diag}(|\mathbf{q}_e|^{r-1}) \dot{\mathbf{q}}_e] \\ &\quad + \mathbf{s}^T \mathbf{u}_s + \mathbf{s}^T \mathbf{D} - \frac{1}{\eta_0} (d - \delta \hat{d}) \dot{\tilde{d}} - \frac{1}{\eta_1} (p - \delta \hat{p}) \dot{\tilde{p}} \end{aligned} \quad (61)$$

Noting that $\mathbf{s}^T \mathbf{s}^\times = [0, 0, 0]$, it has

$$\begin{aligned} \dot{V} &= \mathbf{s}^T [(c_1 \mathbf{q}_e + c_2 \mathbf{F}(\mathbf{q}_e, r) - \mathbf{C} \omega_d)^\times \mathbf{J}_0 \omega + \\ &\quad \mathbf{J}_0 (\omega_e^\times \mathbf{C} \omega_d - \mathbf{C} \dot{\omega}_d) + c_1 \mathbf{J}_0 \dot{\mathbf{q}}_e + c_2 r \mathbf{J}_0 \text{diag}(|\mathbf{q}_e|^{r-1}) \dot{\mathbf{q}}_e] \\ &\quad + \mathbf{s}^T \mathbf{u}_s + \mathbf{s}^T \mathbf{D} - \frac{1}{\eta_0} (d - \delta \hat{d}) \dot{\tilde{d}} - \frac{1}{\eta_1} (p - \delta \hat{p}) \dot{\tilde{p}} \end{aligned} \quad (62)$$

Noting that $(\mathbf{C} \omega_d)^\times (\mathbf{C} \omega_d) = [0, 0, 0]^T$, $\|\mathbf{C}\| = 1$, $\|\mathbf{q}_{e4} + \mathbf{q}_e^\times\| = 1$, it has

$$\begin{aligned} \dot{V} &\leq \|\mathbf{s}\| \|c_1 \mathbf{q}_e + c_2 \mathbf{F}(\mathbf{q}_e, r) - \mathbf{C} \omega_d\| \|\mathbf{J}_0\| \|\omega\| \\ &\quad + \|\mathbf{s}\| \|\mathbf{J}_0\| \|\omega_e^\times \mathbf{C} \omega_d - \mathbf{C} \dot{\omega}_d\| + c_1 \|\mathbf{s}\| \|\mathbf{J}_0\| \|\dot{\mathbf{q}}_e\| \\ &\quad + c_2 r \|\mathbf{s}\| \|\mathbf{J}_0\| \|\mathbf{q}_e\|^{r-1} \|\dot{\mathbf{q}}_e\| + \mathbf{s}^T \mathbf{u}_s + \mathbf{s}^T \mathbf{D} \\ &\quad - \frac{1}{\eta_0} (d - \delta \hat{d}) \dot{\tilde{d}} - \frac{1}{\eta_1} (p - \delta \hat{p}) \dot{\tilde{p}} \\ &\leq \|\mathbf{s}\| (c_1 \|\mathbf{q}_e\| + c_2 \|\mathbf{q}_e\|^r + \|\mathbf{C}\| \|\omega_d\|) \|\mathbf{J}_0\| \|\omega\| \\ &\quad + \|\mathbf{s}\| \|\mathbf{J}_0\| [(\omega - \mathbf{C} \omega_d)^\times \mathbf{C} \omega_d + \|\mathbf{C}\| \|\dot{\omega}_d\|] \\ &\quad + \frac{c_1}{2} \|\mathbf{s}\| \|\mathbf{J}_0\| \|\mathbf{q}_{e4} + \mathbf{q}_e^\times\| \|\omega - \mathbf{C} \omega_d\| \\ &\quad + \frac{c_2}{2} r \|\mathbf{s}\| \|\mathbf{J}_0\| \|\mathbf{q}_e\|^{r-1} \|\mathbf{q}_{e4} + \mathbf{q}_e^\times\| + \mathbf{s}^T \mathbf{u}_s + \mathbf{s}^T \mathbf{D} \\ &\quad - \frac{1}{\eta_0} (d - \delta \hat{d}) \dot{\tilde{d}} - \frac{1}{\eta_1} (p - \delta \hat{p}) \dot{\tilde{p}} \\ &\leq \|\mathbf{s}\| (c_1 \|\mathbf{q}_e\| + c_2 \|\mathbf{q}_e\|^r + \|\omega_d\|) b_J \|\omega\| + \\ &\quad \|\mathbf{s}\| [b_J (\|\omega\| \|\omega_d\| + \|\dot{\omega}_d\|) + \frac{c_1}{2} \|\mathbf{s}\| b_J (\|\omega\| + \|\omega_d\|)] \\ &\quad + \frac{c_2}{2} r \|\mathbf{s}\| b_J \|\mathbf{q}_e\|^{r-1} (\|\omega\| + \|\omega_d\|) + \mathbf{s}^T \mathbf{u}_s + \mathbf{s}^T \mathbf{D} \\ &\quad - \frac{1}{\eta_0} (d - \delta \hat{d}) \dot{\tilde{d}} - \frac{1}{\eta_1} (p - \delta \hat{p}) \dot{\tilde{p}} \\ &= b_J \|\mathbf{s}\| \|\omega\| (c_1 \|\mathbf{q}_e\| + c_2 \|\mathbf{q}_e\|^r + \frac{c_2}{2} r \|\mathbf{q}_e\|^{r-1} + 2 \|\omega_d\| \\ &\quad + \frac{c_1}{2}) + b_J \|\mathbf{s}\| [\|\dot{\omega}_d\| + (\frac{c_1}{2} + \frac{c_2}{2} r \|\mathbf{q}_e\|^{r-1}) \|\omega_d\|] + \\ &\quad \mathbf{s}^T \mathbf{u}_s + \mathbf{s}^T \mathbf{D} - \frac{1}{\eta_0} (d - \delta \hat{d}) \dot{\tilde{d}} - \frac{1}{\eta_1} (p - \delta \hat{p}) \dot{\tilde{p}} \\ &\leq p \|\mathbf{s}\| \|\omega\| + p \|\mathbf{s}\| + \mathbf{s}^T \mathbf{u}_s + \|\mathbf{s}\| [d(1 + \|\omega\| + \|\omega\|^2) \\ &\quad - \frac{1}{\eta_0} (d - \delta \hat{d}) \dot{\tilde{d}} - \frac{1}{\eta_1} (p - \delta \hat{p}) \dot{\tilde{p}}] \end{aligned} \quad (63)$$

By substituting Eqs.(54) and (55) into Eq.(63), it has

$$\begin{aligned}
\dot{V} &\leq p\|\mathbf{s}\|\|\boldsymbol{\omega}\| + p\|\mathbf{s}\| + \mathbf{s}^T \mathbf{u}_s + \|\mathbf{s}\|d(1 + \|\boldsymbol{\omega}\| + \|\boldsymbol{\omega}\|^2) \\
&\quad - (d - \delta\hat{d})\|\mathbf{s}\|d(1 + \|\boldsymbol{\omega}\| + \|\boldsymbol{\omega}\|^2) + \epsilon_0\hat{d}(d - \delta\hat{d}) \\
&\quad - (p - \delta\hat{p})\|\mathbf{s}\|(1 + \|\boldsymbol{\omega}\|) + \epsilon_1\hat{p}(p - \delta\hat{p}) \\
&\leq -\delta\mathbf{s}^T \mathbf{u} + \delta\hat{d}\|\mathbf{s}\|\Phi_0 + \epsilon_0\hat{d}(d - \delta\hat{d}) \\
&\quad + \delta\hat{p}\|\mathbf{s}\|\Phi_1 + \epsilon_1\hat{p}(p - \delta\hat{p})
\end{aligned} \tag{64}$$

When $\|\mathbf{s}\| \geq \sigma$, the following result holds by substituting \mathbf{u} into Eq.(64)

$$\begin{aligned}
\dot{V} &\leq -\delta k_1 \mathbf{s}^T \mathbf{s} - \delta k_2 \mathbf{s}^T \mathbf{F}(\mathbf{s}) - \delta \mathbf{s}^T \mathbf{u}_{ad} + \delta \hat{d} \|\mathbf{s}\| \Phi_0 \\
&\quad + \epsilon_0 \hat{d} (d - \delta \hat{d}) + \delta \hat{p} \|\mathbf{s}\| \Phi_1 + \epsilon_1 \hat{p} (p - \delta \hat{p}) \\
&= -\delta k_2 \|\mathbf{s}\|^{r+1} + \epsilon_0 \hat{d} (d - \delta \hat{d}) + \epsilon_1 \hat{p} (p - \delta \hat{p}) \\
&= -\delta k_2 \|\mathbf{s}\|^{r+1} + \epsilon_0 \tilde{d} \hat{d} + \epsilon_1 \tilde{p} \hat{p}
\end{aligned} \tag{65}$$

For any $n_0 > 1/2$, one has

$$\begin{aligned}
\epsilon_0 \tilde{d} \hat{d} &= \frac{\epsilon_0}{\delta} (d \tilde{d} - \tilde{d}^2) \\
&\leq \frac{\epsilon_0}{\delta} (-\tilde{d}^2 + \frac{1}{2n_0} \tilde{d}^2 + \frac{n_0}{2} d^2) \\
&= \frac{-\epsilon_0(2n_0 - 1)}{\delta n_0} \tilde{d}^2 + \frac{\epsilon_0 n_0}{2\delta} d^2
\end{aligned} \tag{66}$$

and it results in

$$\frac{\epsilon_0(2n_0 - 1)}{\delta n_0} \tilde{d}^2 + \epsilon_0 \tilde{d} \hat{d} \leq \frac{\epsilon_0 n_0}{2\delta} d^2 \tag{67}$$

Let $\gamma = \frac{r+1}{2}$, then $0.5 < \gamma < 1$. It has

$$\left(\frac{\epsilon_0(2n_0 - 1)}{\delta n_0} \tilde{d}^2 \right)^\gamma \leq \frac{\epsilon_0(2n_0 - 1)}{\delta n_0} \tilde{d}^2 \tag{68}$$

for $\frac{\epsilon_0(2n_0 - 1)}{\delta n_0} \tilde{d}^2 \geq 1$, and

$$\left(\frac{\epsilon_0(2n_0 - 1)}{\delta n_0} \tilde{d}^2 \right)^\gamma \leq 1 \tag{69}$$

when $\frac{\epsilon_0(2n_0 - 1)}{\delta n_0} \tilde{d}^2 \leq 1$. Thus, it always has

$$\left(\frac{\epsilon_0(2n_0 - 1)}{\delta n_0} \tilde{d}^2 \right)^\gamma \leq \frac{\epsilon_0(2n_0 - 1)}{\delta n_0} \tilde{d}^2 + 1 \tag{70}$$

thus yielding

$$\left(\frac{\epsilon_0(2n_0 - 1)}{\delta n_0} \tilde{d}^2 \right)^\gamma + \epsilon_0 \tilde{d} \hat{d} \leq \frac{\epsilon_0(2n_0 - 1)}{\delta n_0} \tilde{d}^2 + \epsilon_0 \tilde{d} \hat{d} + 1 \tag{71}$$

From Eq.(67), it has

$$\left(\frac{\epsilon_0(2n_0 - 1)}{\delta n_0} \tilde{d}^2 \right)^\gamma + \epsilon_0 \tilde{d} \hat{d} \leq \frac{\epsilon_0 n_0}{2\delta} d^2 + 1 \tag{72}$$

Then, the following inequality holds

$$\epsilon_0 \tilde{d} \hat{d} \leq \frac{\epsilon_0 n_0}{2\delta} d^2 + 1 - \left(\frac{\epsilon_0(2n_0 - 1)}{\delta n_0} \tilde{d}^2 \right)^\gamma \tag{73}$$

Similarly, for any $n_1 > 1/2$, it has

$$\epsilon_1 \tilde{p} \hat{p} \leq \frac{\epsilon_1 n_1}{2\delta} p^2 + 1 - \left(\frac{\epsilon_1(2n_1 - 1)}{\delta n_1} \tilde{p}^2 \right)^\gamma \tag{74}$$

Thus, the derivative of V is

$$\begin{aligned}
\dot{V} &\leq -\delta k_2 \|\mathbf{s}\|^{r+1} + \frac{\epsilon_0 n_0}{2\delta} d^2 + 1 - \left(\frac{\epsilon_0(2n_0 - 1)}{\delta n_0} \tilde{d}^2 \right)^\gamma \\
&\quad + \frac{\epsilon_1 n_1}{2\delta} p^2 + 1 - \left(\frac{\epsilon_1(2n_1 - 1)}{\delta n_1} \tilde{p}^2 \right)^\gamma
\end{aligned} \tag{75}$$

Define

$$\lambda := \frac{k_2 2^\gamma}{\|\mathbf{J}_0\|^\gamma} \tag{76}$$

$$\eta := \frac{\epsilon_0 n_0}{2\delta} d^2 + \frac{\epsilon_1 n_1}{2\delta} p^2 + 2 \tag{77}$$

η_0 and η_1 can be designed as

$$\eta_0 = \frac{n_0 \lambda}{\epsilon_0(2n_0 - 1)} \tag{78}$$

$$\eta_1 = \frac{n_1 \lambda}{\epsilon_1(2n_1 - 1)} \tag{79}$$

Considering Eqs.(75)-(79), it has

$$\begin{aligned}
\dot{V} &\leq -\lambda \left[\left(\frac{1}{2} \mathbf{s}^T \mathbf{J}_0 \mathbf{s} \right)^\gamma + \left(\frac{1}{2\eta_0 \delta} \tilde{d}^2 \right)^\gamma + \left(\frac{1}{2\eta_1 \delta} \tilde{p}^2 \right)^\gamma \right] + \eta \\
&= -\lambda V^\gamma + \eta
\end{aligned} \tag{80}$$

According to Lemma 1, the following result can be achieved in finite time

$$V^\gamma \leq \frac{\eta}{\lambda(1 - \kappa)}, \kappa \in (0, 1) \tag{81}$$

As a result, the trajectory of the sliding surface \mathbf{s} is bounded in finite time T_1 , such that

$$\lim_{t \rightarrow T_1} \mathbf{s}(t) \in \{\mathbf{s} : \|\mathbf{s}\| \leq \Gamma\} \tag{82}$$

where $\Gamma = \frac{\eta \sqrt{2\|\mathbf{J}_0\|}}{\lambda(1 - \kappa)}$, and

$$T_1 \leq \frac{V_0^{(1-\gamma)}}{\lambda \kappa (1 - \gamma)} \tag{83}$$

where V_0 is the initial state of V .

It can be concluded that the trajectory of the closed-loop system of Eqs. (30) and (31) can be driven onto area of $\|\mathbf{s}\| \leq \Gamma$ in finite time T_1 .

In the case of $\|\mathbf{s}\| < \sigma$, reaching the sliding surface $\mathbf{s} = 0$ in finite time cannot be guaranteed. According to Zhong et al. (2016), $\sigma \leq \Gamma$ can always hold by properly choosing σ . In this way, with the proposed controller, the system states would converge to the small neighborhood $\|\mathbf{s}\| \leq \Gamma$ in finite time.

3.3 Actuator Allocation

The moving distances of sliding masses and rotational angle of RSB are solved from the designed control law. According to Eq.(3), the actuators' solutions can be described as

$$\alpha_{bc} = \frac{3\sqrt{2}}{l_b(F_s + \varepsilon)} \left[\mathbf{u}_{sx} + \frac{m_r}{M} (F_z d_{yc} - F_y d_{zc}) \right] \tag{84}$$

$$d_{yc} = -\frac{\mathbf{u}_{sz} M}{m_r(F_x + \varepsilon)} \tag{85}$$

$$d_{zc} = \frac{\mathbf{u}_{sy} M}{m_r(F_x + \varepsilon)} \tag{86}$$

where u_{sx} , u_{sy} , and u_{sz} are control torques along three axes and hold $\mathbf{u}_s = [u_{sx}, u_{sy}, u_{sz}]^T$. ε is a small positive variable applied to avoid the singularity when $\cos \alpha_s = 0$.

The dynamics of the actuators are considered as (Wie and Murphy (2007))

$$T_a \dot{\alpha}_b + \alpha_b = \alpha_{bc} \quad (87)$$

$$T_m \dot{d}_y + d_y = d_{yc} \quad (88)$$

$$T_m \dot{d}_z + d_z = d_{zc} \quad (89)$$

where T_a and T_m are the time constants of the RSB and sliding masses.

4. SIMULATION

The parameters of a $40\text{m} \times 40\text{m}$ solar sail taken from Wie and Murphy (2007) are shown in Table 1. Because the Sun-line law has important application in orbit design of solar sail, e.g., Heiligers et al. (2015), it is taken as the desired attitude to prove the effectiveness of our proposed attitude control strategy. It requires the sail's normal vector to track the sunlight vector, i.e., α_s is asked to converge to 0. The motion of the sunlight vector can be described in the inertia frame as

$$\mathbf{r}_{sI} = [\cos(\omega_s t), -\sin(\omega_s t), 0]^T \quad (90)$$

The initial attitude angular error is set to 35deg, which can be described by quaternion $\mathbf{Q}_0 = [0, 0, 0.2588, 0.9659]^T$, while the initial angular velocity is $\boldsymbol{\omega}_0 = [0, 0, 0]^T$. In addition, $\rho_s = 0.9$ and $\rho_d = 0.1$. The control parameters are designed as $c_1 = 0.01$, $c_2 = 0.001$, $g = 9$, $h = 17$, $n_0 = n_1 = 0.8$, $\epsilon_0 = \epsilon_1 = 0.0001$, $k_1 = 0.1$, $k_2 = 0.1$, $\sigma = 0.001$, $\varepsilon = 0.0001$.

Figs.3 and 4 give the errors in attitude quaternion and angular velocity. To illustrate the result of attitude tracking, the Sun angle is shown in Fig. 5. It can be seen that the angle converges to the neighborhood of zero in less than 1 h with an error of 0.7 deg. For a 35-degree attitude maneuver, the convergence in Wie and Murphy (2007) took about 2h. Thus, the control process of our proposed control system is relatively fast.

Fig.6 and 7 show the time histories of the changing inertia and the SRP disturbance torque. It can be noted that the inertia changes a lot compared to its principal part due to the large movements of the sliding masses. The SRP disturbance torque is time varying because of the attitude adjustment.

Fig.8 illustrates the time histories of the state-dependent torque saturation. Figs.9-11 present the proposed control law and the actual control torques generated by the actuators along three axes. In each figure, the red dashed lines indicate the upper and lower bounds of each axis as shown in Fig.8. The control torques for the roll and pitch axes are within their saturation limits. For the yaw axis, at the beginning of simulation, the saturation is soon reached to make full use of the control effort. Then, with the drop of attitude tracking error, the designed control effort decreases a lot. At last, small torques are still required to counteract the disturbance. The time-delay properties of the actuators' dynamics result in errors between the designed control effort and the actual torque.

Fig.12 displays the rotational angle of the RSB and the positions of two sliding masses. The saturation of d_y also appears following the trend of control torque along yaw axis. Additionally, d_z and α_s both vary within their affordable values. As the control efforts decrease, the oscillations of α_s , d_y , and d_z also decay. The actuators'

variables are almost fixed at certain values to generate control torque for disturbance rejection and uncertainty compensation.

Table 1. The parameters of solar sail

Parameter	Value
l_b	1m
α_{bm}	30deg
ι_{0y}	0.1m
ι_{0z}	0.1m
A_s	1400m ²
T_a	560s
M	150kg
d_m	28m
$[J_{x0}, J_{y0}, J_{z0}]$	[4332, 2116, 2116]kgm ²
ω_s	1.5178×10^{-4} deg/s
P	4.563×10^{-6} N/m ²
T_m	560s

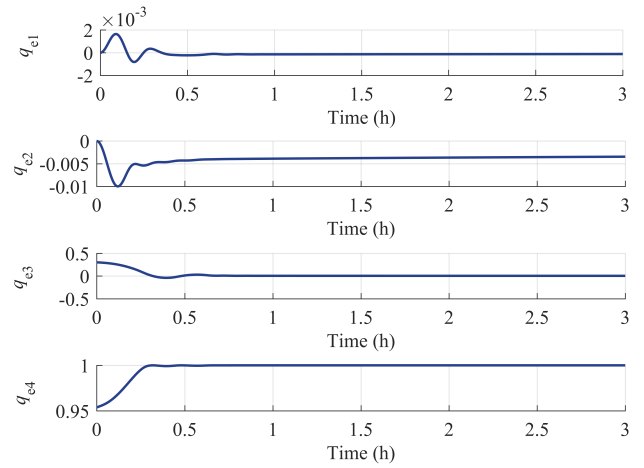


Fig. 3. Attitude quaternion error

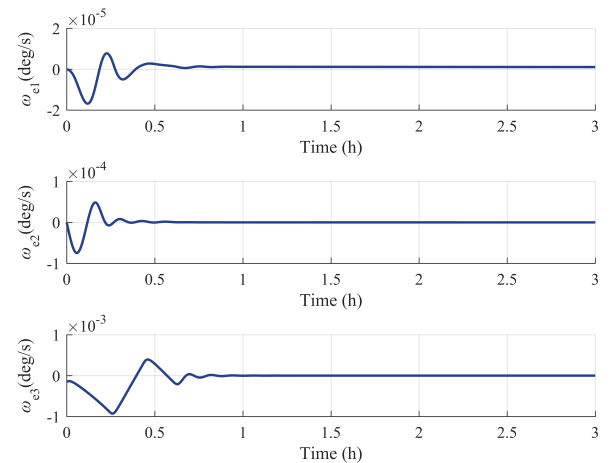


Fig. 4. Attitude angular velocity error

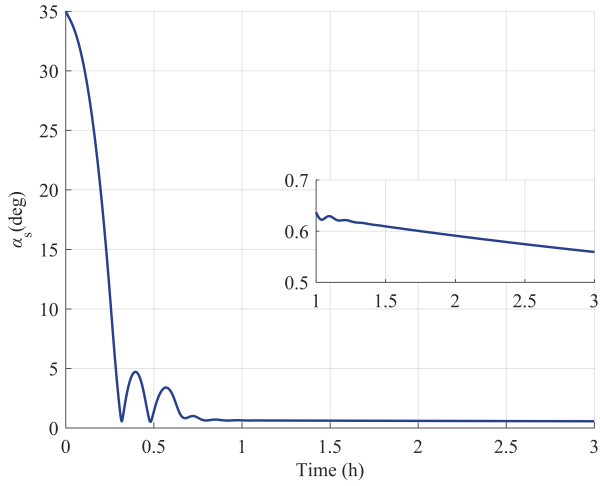


Fig. 5. Sun angle

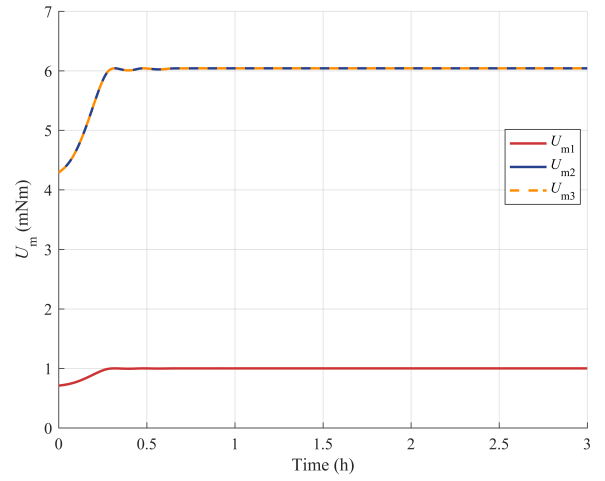


Fig. 8. Torque saturation

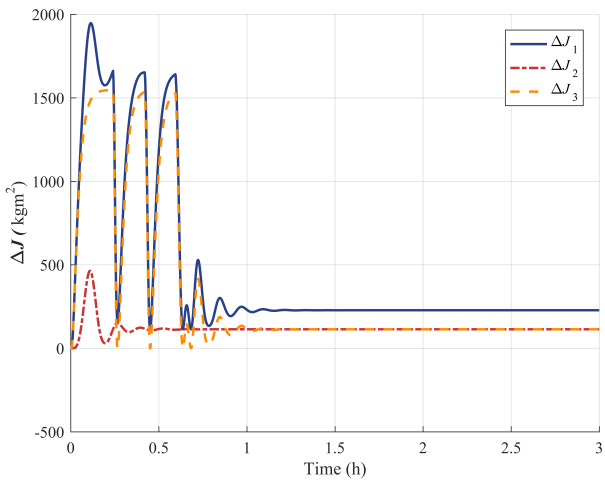


Fig. 6. Changing Inertia

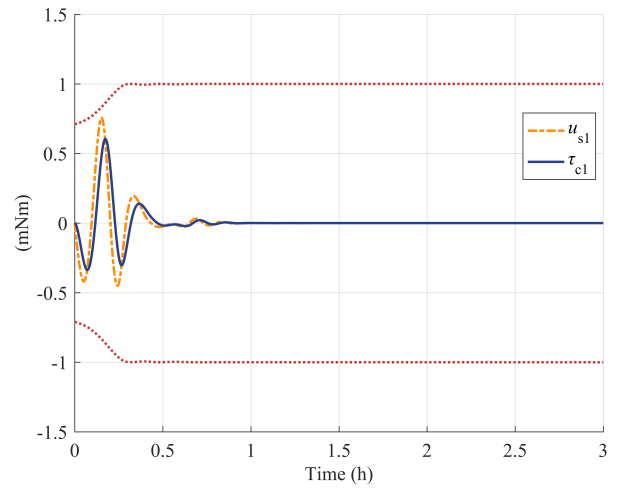


Fig. 9. Control efforts of roll axis

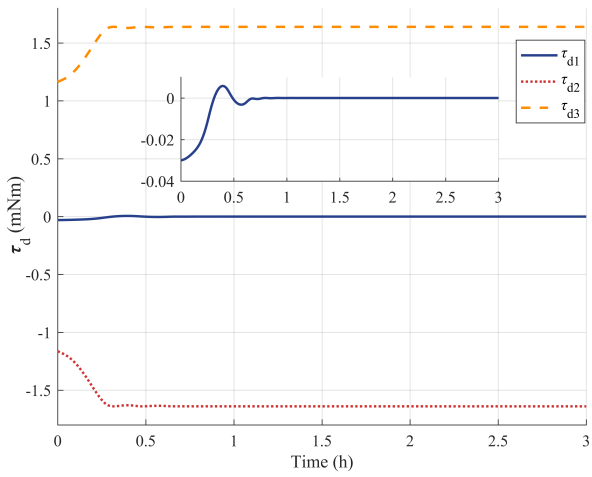


Fig. 7. SRP disturbance torque

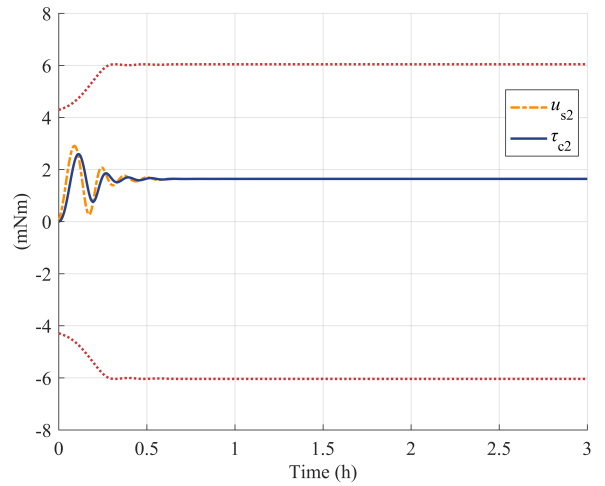


Fig. 10. Control efforts of pitch axis

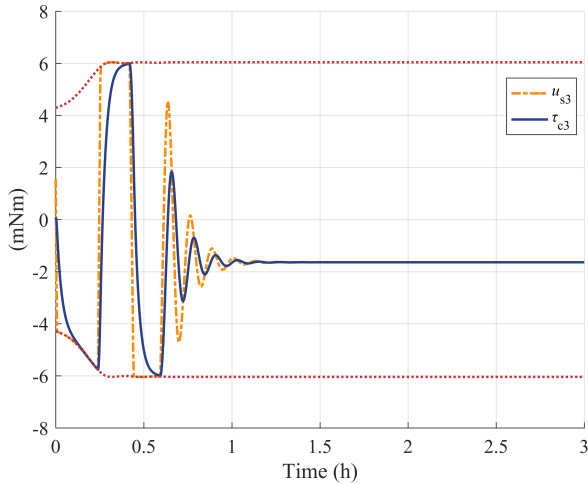


Fig. 11. Control efforts of yaw axis

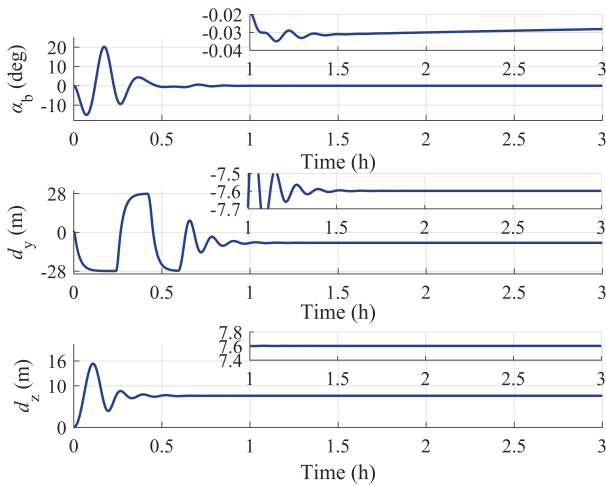


Fig. 12. Time histories of the actuators' motions

In conclusion, the desired attitude is successfully tracked in finite time under the proposed control strategy in the presence of actuators dynamics, changing inertia, unknown SRP disturbance, and torque constraints caused by actuator saturation and attitude maneuver.

5. CONCLUSION

In this paper, a three-axis attitude tracking controller is designed for a solar sail equipped with sliding masses and RSB in the presence of uncertain inertia, unknown SRP disturbance and torque constraints caused by actuator saturation and attitude maneuver. The model of the control torque with respect to attitude angle is established. A state-dependent torque saturation is proposed to deal with the torque constraints. Effective adaptive laws are proposed to handle the uncertain and unknown information of inertia, SRP disturbance, and torque constraints. The proposed control strategy successfully stabilizes the closed-loop attitude control system in finite time, where the state-dependent saturation of control torque are fully used, and

achieves a relatively fast attitude tracking control for solar sail.

REFERENCES

- Adeli, S.N., Lappas, V.J., and Wie, B. (2011). A scalable bus-based attitude control system for solar sails. *Advances in Space Research*, 48(11), 1836–1847.
- Baculi, J. and Ayoubi, M.A. (2017). Fuzzy attitude control of solar sail via linear matrix inequalities. *Acta Astronautica*, 138, 233–241.
- Bassetto, M., Niccolai, L., Boni, L., Mengali, G., Quarta, A.A., Circi, C., Pizzurro, S., Pizzarelli, M., Pellegrini, R.C., and Cavallini, E. (2022). Sliding mode control for attitude maneuvers of helianthus solar sail. *Acta Astronautica*, 198, 100–110.
- Bolle, A. and Circi, C. (2008). Solar sail attitude control through in-plane moving masses. *Proceedings of the Institution of Mechanical Engineers Part G Journal of Aerospace Engineering*, 222(1), 81–94.
- Carzana, L., Visser, P., and Heiligers, J. (2022). Locally optimal control laws for earth-bound solar sailing with atmospheric drag. *Aerospace Science and Technology*, 127, 107666.
- Eldad, O. and Lightsey, E. (2015). Propellantless attitude control of a nonplanar solar sail. *Journal of Guidance, Control, and Dynamics*, 38(8), 1531–1534.
- Gong, S. and Li, J. (2015). A new inclination cranking method for a flexible spinning solar sail. *IEEE Transactions on Aerospace and Electronic Systems*, 51(4), 2680–2696.
- Hassanpour, S. and Damaren, C.J. (2018). Linear structural dynamics and tip-vane attitude control for square solar sails. *Journal of Guidance Control and Dynamics*, 41(11), 2401–2415.
- Hassanpour, S. and Damaren, C.J. (2019). Collocated attitude and vibrations control for square solar sails with tip vanes. *Acta Astronautica*, 166, 482–492.
- Heiligers, J., Hiddink, S., Noomen, R., and McInnes, C.R. (2015). Solar sail lyapunov and halo orbits in the earth moon three body problem. *Acta Astronautica*, 116, 25–35.
- Hu, Q. and Tan, X. (2017). Finite time fault tolerant spacecraft attitude control with torque saturation. *Journal of Guidance Control and Dynamics*, 40(10), 2524–2537.
- Huang, H. and Zhou, J. (2019). Solar sailing cubesat attitude control method with satellite as moving mass. *Acta Astronautica*, 159, 331–341.
- Lian, X., Liu, J., Wang, C., Yuan, T., and Cui, N. (2018). Rbf network based adaptive sliding mode control for solar sails. *Aircraft Engineering and Aerospace Technology*, 90(8), 1180–1191.
- Lu, K., Xia, Y., and Fu, M. (2013). Controller design for rigid spacecraft attitude tracking with actuator saturation. *Information Sciences*, 220, 343–366.
- Macdonald, M. and Hughes, G.W. (2006). Solar polar orbiter: A solar sail technology reference study. *Journal of Spacecraft and Rockets*, 43(5), 960–972.
- Mu, J., Gong, S., and Li, J. (2015). Coupled control of reflectivity modulated solar sail for geosail formation flying. *Journal of Guidance Control and Dynamics*, 38(4), 740–751.

- Niccolai, L., Quarta, A.A., and Mengali, G. (2017). Analytical solution of the optimal steering law for non-ideal solar sail. *Aerospace Science and Technology*, 62, 11–18.
- Orphee, J., Diedrich, B., Stiltner, B., and Heaton, A. (2016). Solar sail attitude control system for the nasa near earth asteroid scout mission. *Solar Sail Attitude Control System for the NASA Near Earth Asteroid Scout Mission, NASA Technical Report*.
- Pengyuan, Z., Chenchen, W., and Yangmin, L. (2022). Design and application of solar sailing: A review on key technologies. *Chinese Journal of Aeronautics*.
- Quarta, A.A., Bianchi, C., Niccolai, L., and Mengali, G. (2022). Solar sail-based v-infinity leveraging missions from elliptic orbit. *Aerospace Science and Technology*, 130, 107922.
- Romagnoli, D. and Oehlschlagel, T. (2011). High performance two degrees of freedom attitude control for solar sails, advances in space research. *Advances in Space Research*, 48(11), 1869–1879.
- Scholz, C., Romagnoli, D., Dachwald, B., and Theil, S. (2011). Performance analysis of an attitude control system for solar sails using sliding masses. *Advances in Space Research*, 48(11), 1822–1835.
- Spencer, D.A., Betts, B., Bellardo, J.M., Diaz, A., Plante, B., and Mansell, J.R. (2021). The lightsail 2 solar sailing technology demonstration. *Advances in Space Research*, 67(9), 2878–2889.
- Tamakoshi, D. and Kojima, H. (2017). Solar sail orbital control using reflectivity variations near the earth-moon l2 point. *Journal of Guidance Control Dynamics*, 41(2), 417–430.
- Thomas, S., Paluszek, M., Wie, B., and Murphy, D. (2005). Aocs performance and stability validation for large flexible solar sail spacecraft. *41st AIAA/ASME/SAE/ASEE Joint Propulsion Conference & Exhibit*, 3926.
- Tian, J., Gong, S., Mu, J., Li, J., Wang, T., and Qian, W. (2016). Switch programming of reflectivity control devices for the coupled dynamics of a solar sail. *Advances in Space Research*, 57(5), 1147–1158.
- Wie, B. and Murphy, D. (2007). Solar-sail attitude control design for a flight validation mission. *Journal of Spacecraft and Rockets*, 44(4), 809–821.
- Wu, L. and Guo, Y. (2020). Effect of attitude control on a periodic orbit maintenance of solar sail in earth-moon circular restricted 3-body problem. *2020 39th Chinese Control Conference (CCC)*, 569–574.
- Wu, L., Guo, Y., and Guo, J. (2018). Attitude control for solar-sail using rotating panel-sliding mass actuator. *Harbin Inst. Technol*, 50(9), 141–146.
- Yoshimura, Y., Matsushita, Y., Arakawa, R., and Hanada, T. (2020). Light curve approximation using an attitude model of solar sail spacecraft. *Journal of Guidance, Control, and Dynamics*, 10(43), 1960–1966.
- Zhong, C., Wu, L., Guo, J., Guo, Y., and Chen, Z. (2016). Robust adaptive attitude manoeuvre control with finite-time convergence for a flexible spacecraft. *Transactions of the Institute of Measurement and Control*, 40(2), 425–435.
- Zhu, Z., Xia, Y., and Fu, M. (2011). Attitude stabilization of rigid spacecraft with finite time convergence. *International Journal of Robust and Nonlinear Control*, 21(6), 686–702.
- Zhu, Z. and Guo, Y. (2017). Adaptive fault tolerant attitude tracking control for spacecraft formation with unknown inertia. *International Journal of Adaptive Control and Signal Processing*, 32(1), 13–26.
- Zhu, Z., Guo, Y., and Gao, Z. (2019). Adaptive finite time actuator fault tolerant coordinated attitude control of multispacecraft with input saturation. *International Journal of Adaptive Control and Signal Processing*, 33(4), 644–663.